A&A 658, A150 (2022)
https://doi.org/10.1051/0004-6361/202142287

Astronomy & Astrophysics

The trans/cis ratio of formic (HCOOH) and thioformic (HC(O)SH) acids in the interstellar medium

J. García de la Concepción[1], L. Colzi[1,2], I. Jiménez-Serra[1], G. Molpeceres[3], J. C. Corchado[4], V. M. Rivilla[1,2], J. Martín-Pintado[1], M. T. Beltrán[2], and C. Mininni[5]

[1] Centro de Astrobiología (CSIC-INTA), Ctra. de Ajalvir Km. 4, Torrejón de Ardoz, 28850 Madrid, Spain
e-mail: jgarcia@cab.inta-csic.es
[2] INAF-Osservatorio Astrofisico di Arcetri, Largo E. Fermi 5, 50125 Florence, Italy
[3] Institute for Theoretical Chemistry, University of Stuttgart, Pfaffenwaldring 55, 70569 Stuttgart, Germany
[4] Departamento de Ingeniería Química y Química Física, Facultad de Ciencias, and ICCAEx, Universidad Extremadura, Badajoz, Spain
[5] INAF-IAPS, via del Fosso del Cavaliere 100, 00133 Roma, Italy

Received 23 September 2021 / Accepted 28 October 2021

ABSTRACT

Context. Observations of the different isomers of molecules in the interstellar medium (ISM) have revealed that both low- and high-energy isomers can be present in space despite the low temperature conditions. It has been shown that the presence of these isomers may be due to tunneling effects.

Aims. We carried out a theoretical study of the cis–trans isomerization reactions of two astrophysically relevant acids, formic acid (HCOOH) and thioformic acid (HC(O)SH), where the latter has recently been discovered in space. We also searched for these molecules towards the hot core G31.41+0.31 to compare their abundances with the expected theoretical isomerization results.

Methods. We employed high-level ab initio calculations to study the reaction rate constants of the isomerization reactions. We used the canonical variational transition state theory with the multidimensional small curvature tunneling approximation in the temperature range of 10–400 K. Moreover, we used the spectrum obtained from the ALMA 3mm spectral survey GUAPOS (GUAPOS: G31 Unbiased ALMA sPectral Observational Survey), with a spectral resolution of ∼0.488 MHz and an angular resolution of 1.″2×1.″2 (∼4500 au), to derive column densities of HCOOH and HC(O)SH towards G31.41+0.31.

Results. Our results demonstrate that these isomerizations are viable in the conditions of the ISM due to ground-state tunneling effects, which allow the system to reach the thermodynamic equilibrium at moderately low temperatures. At very low temperatures ($T_{\rm kin}$ ∼ 10 K), the reaction rate constants for the cis-to-trans isomerizations are very small, which implies that the cis isomers should not be formed under cold ISM conditions. This is in disagreement with observations of the cis/trans isomers of HCOOH in cold cores where the cis isomer is found to be ∼5–6% the trans isomer. At high temperatures (∼150–300 K), our theoretical data not only match the observed behavior of the trans/cis abundance ratios for HCOOH (the cis form is undetected), but they support our tentative detection of the trans and – for the first time in the insterstellar medium – the cis isomer of HC(O)SH towards the hot molecular core G31.41+0.31 (with a measured trans/cis abundance ratio of ∼3.7).

Conclusions. While the trans/cis ratio for HC(O)SH in the ISM depends on the relative stability of the isomers, the trans/cis ratio for HCOOH cannot be explained by isomerization, and is determined by other competitive chemical processes.

Key words. ISM: molecules – ISM: individual objects: G31.41+0.31 – stars: formation – methods: numerical – methods: observational – astrochemistry

1. Introduction

The detection of isomers in the interstellar medium (ISM) has triggered efforts in astrophysics to gain insight into the formation path of these species. As an illustration, let us consider the different values of the E/Z isomer ratios of imines such as cyanomethanimine, ethanamine, and acetylenimine measured across different environments of the ISM (Loomis et al. 2013; Rivilla et al. 2018; Bizzocchi et al. 2020). Several theories have been proposed to explain the different observed E/Z ratios. The most popular approach considers that the different isomers should be formed through competitive chemical routes that selectively lead to the observed ratio (Puzzarini 2015; Quan et al. 2016; Balucani et al. 2018; Melli et al. 2018; Baiano et al. 2020; Bizzocchi et al. 2020; Lupi et al. 2020; Shingledecker et al. 2020). This approach implicitly assumes that the thermodynamic equilibrium between the isomers cannot be reached under the conditions of the ISM due to the high energy barriers of the isomerization reactions (∼25–30 kcal mol^{-1}, García de la Concepción et al. 2021; Vazart et al. 2015; Balucani et al. 2018; Baiano et al. 2020). However, in previous works, the quantum tunneling corrections to the rate coefficients were carried out using a one-dimensional treatment (see Sect. 2.3 in Bao & Truhlar 2017). More recently, we demonstrated that multidimensional treatment of this quantum effect (e.g., where all the degrees of freedom of the molecule are considered in the tunneling process) increases the transmission coefficients by several orders of magnitude (García de la Concepción et al. 2021). As a result, the ratio between the E/Z isomers of cyanomethanimine, ethanamine, and propinimine depends on the isomer relative stability because the thermodynamic equilibrium can be reached in the ISM thanks to

ground-state quantum tunneling effects (García de la Concepción et al. 2021).

Recently, the trans isomer of thioformic acid, t-HC(O)SH, was discovered in the ISM (with an abundance of 1.2×10^{-10}; Rodríguez-Almeida et al. 2021). This species was found toward the giant molecular cloud G+0.693-0.027 located in the Galactic center (with a kinetic temperature of $T_{\rm kin}(\sim)150$ K), where only the trans isomer could be detected (the derived upper limit abundance of the cis isomer, c-HC(O)SH, is $\leq 0.2 \times 10^{-10}$; Rodríguez-Almeida et al. 2021). The selective formation of t-HC(O)SH on dust grains has been found to be very efficient through the hydrogenation of OCS in ices (Molpeceres et al. 2021). However, this is the only detection of this species in the ISM so far (Rodríguez-Almeida et al. 2021), and it remains unknown whether it could be present toward other sources, either in its trans isomeric form or in both trans and cis forms.

Likewise, the trans isomer of the formic acid, t-HCOOH, has been widely detected in the ISM, in cold pre-stellar cores such as L1544 or L183 (Vastel et al. 2014; Lattanzi et al. 2020) and low-mass protostars (e.g., Yang et al. 2021; Maureira et al. 2020; Manigand et al. 2020; van Gelder et al. 2020), to protoplanetary disks (Favre et al. 2018; Lee et al. 2019) and massive star-forming regions both in the Galactic disk (e.g., Rivilla et al. 2017a; Gieser et al. 2019; Peng et al. 2019) and in the Galactic center (e.g., Belloche et al. 2013; Li et al. 2020; Rodríguez-Almeida et al. 2021). Unlike t-HCOOH, the cis isomer, c-HCOOH has been only found towards sources such as the photon-dominated region (PDR) of the Orion Bar (with a trans/cis abundance ratio of 2.8; Cuadrado et al. 2016), and the dense cold molecular clouds ($T_{\rm kin} \sim 10$ K) L483 (Agúndez et al. 2019) and B5 (Taquet et al. 2017), with a trans/cis ratio of ∼16.7. For the Orion Bar PDR, high-energy uv photons excite the molecule of HCOOH to the first singlet excited state, and then the deactivation of the excited state to the ground state of the cis and trans isomers enables the observations of both conformers. For the cold dense clouds, there are no incident uv photons, but there are secondary uv fields produced by the relaxation of hydrogen from high excited states that can be generated by cosmic rays. This latter process could also alter the trans/cis isomer ratio. This questions whether the observed trans/cis ratios are due to a temperature effect that would allow the formation of the cis isomer, or whether the systems are in thermodynamic equilibrium as observed for imines. The prevalence of one isomer over the other as a function of the $T_{\rm kin}$ could be of great importance to better understand the chemistry of the ISM.

It is well known that simple carboxylic acids like HCOOH acid can isomerize from the least stable isomer (cis) to the most stable (trans) through quantum tunneling at very low temperatures (Pettersson et al. 2002; Maçôas et al. 2005; Domanskaya et al. 2009; Tsuge & Khriachtchev 2014). Photoisomerization mechanisms have been observed for isomers of thioformic acids (Lignell et al. 2021). However, ground state quantum tunneling effects have not yet been explored for thiocarboxylic acids, like HC(O)SH. In this study, we carried out a theoretical analysis of the isomerization reaction of the HCOOH and HC(O)SH acids at interstellar temperatures ($T_{\rm kin}$ = 10–400 K) in vacuum, with the aim of understanding whether or not the prevalence of one isomer over the other in the ISM is due to an isomerization transformation. To account for the quantum tunneling effect, which is very important especially at low temperatures, we selected the multidimensional small curvature tunneling (SCT) approximation, which has been demonstrated to give much higher transmission coefficients than other conventional monodimensional treatments (García de la Concepción et al. 2021).

In Sect. 2, we describe the computational details used in this work and in Sect. 3 we explain the results obtained, both the electronic structure calculations and the kinetic results. In Sect. 4, we present the detection of t-HCOOH and the tentative detection of c-HC(O)SH and t-HC(O)SH toward the massive hot core G31.41+0.31 (G31 hereafter). In Sect. 5, we compare the trans/cis ratios found toward several astronomical sources with our theoretical predictions. In Sect. 6, we give the conclusions of this work.

2. Computational details

2.1. Electronic structure calculations

All the stationary points were optimized without constraints at the double-hybrid B2PLYP (Grimme 2006) with the dispersion-corrected D3(BJ) (Grimme et al. 2010, 2011) method in combination with the Dunning's triple-zeta correlation-consistent basis set, augmented with diffuse functions for all atoms (aug-cc-pVTZ) (Dunning Jr. 1989; Kendall et al. 1992). The same level of theory was used to compute frequency calculations in order to characterize the stationary points, which showed none and one imaginary frequency for the energy minima and saddle points, respectively. To improve the level of theory, we corrected the electronic energies of the optimized geometries at B2PLYP-D3(BJ)/aug-cc-pVTZ with the CCSD(T)-F12 method (Adler et al. 2007; Knizia et al. 2009) which includes correlated basis functions and the RI approach for the correlation integrals (Feyereisen et al. 1993). As auxiliary and special orbital basis set, the cc-pVTZ-F12-CABS and cc-pVTZ-F12 were used in combination with the augmented quadruple zeta aug-cc-pVQZ for the correlation and coulomb fitting. Finally, we corrected the electronic energies by computing the anharmonic zero-point energy (ZPE) of the stationary points within vibrational perturbative theory to second order (Barone 2004). The relative energies are given with respect to the least stable isomer (cis). In order to validate the choice of the double-hybrid method we also optimized all the stationary points for HCOOH with the CCSD(T)-F12 method in conjunction with the cc-pVTZ-F12-CABS and cc-pVTZ-F12 basis set and the aug-cc-pVTZ for the correlation and coulomb fitting (see Appendix A). We also computed the harmonic frequencies at the same level of theory, finding one and none imaginary frequencies for the saddle point and energy minima respectively. The comparison between these two methods shows that the B2PLYP-D3(BJ) is suitable for quantitative investigations, because both the relative energies and the geometries of the stationary points are almost identical (see Tables A.1 and A.2 and Fig. A.1). The NBO second-order perturbation theory was used to study the orbital interactions. For the geometry optimization with the double-hybrid functional, and the correction of the electronic energies with the coupled-cluster method, the Gaussian 16 (Frisch et al. 2016) and ORCA (Neese 2012; Neese et al. 2020) software packages were employed respectively. For visualization of the geometries and the orbital isosurfaces we used the Cylview (Legault 2009) and Chimera (Pettersen et al. 2004) softwares respectively.

2.2. Kinetics calculations

We used the canonical variational transition state theory (CVT; Bao & Truhlar 2017) to compute rate constants with the small curvature tunneling approximation (SCT) in the temperature (T) range of 10–400 K. The expression for the unimolecular rate

constants is given by

$$K^{\mathrm{CVT/SCT}}(T) = \kappa^{\mathrm{SCT}}\Gamma^{\mathrm{CVT}}\frac{K_{\mathrm{B}}T}{h}\frac{Q^{\mathrm{VT}}}{Q^{R}}e(-E^{\mathrm{VT}}/RT), \quad (1)$$

where R is the ideal gas constant; κ^{SCT} is the small curvature multidimensional tunneling transmission coefficient; Γ^{CVT} is the canonical variational transition state recrossing coefficient, which is given by $K^{\mathrm{CVT}}/K^{\mathrm{TST}}$, where K^{TST} is the rate coefficient of the conventional transition state theory, whereas K^{CVT} is the rate coefficient of the canonical variational transition state theory; K_{B} is the Boltzmann constant and h is the Planck constant; Q^{VT} and Q^{R} are the total partition functions of the variational transition state and the reactant, respectively; and E^{VT} is the potential energy of the variational transition state. The energies of the minimum energy path (MEP) obtained with the double-hybrid B2PLYP-D3(BJ)/aug-cc-pVTZ were corrected with the coupled cluster method mentioned in Sect. 2.1 using the interpolated single-point energies (ISPE) algorithm (Chuang et al. 1999). The rate coefficient calculations were carried out with the Pilgrim software (Ferro-Costas et al. 2020).

Finally, we note that "forward pathway" (i.e., from $S < 0$ to $S > 0$, with S being the reaction coordinate in Bohr) hereafter refers to the movement along the reaction path from the cis isomer to the trans isomer. For simplicity, the forward cis to trans rate constants are denoted as K_1 and the backward trans to cis as K_{-1}.

3. Results

3.1. Stationary points and stereoelectronic effects

The isomerization reaction of the HC(O)SH involves the rotation of the O–C–S–H dihedral angle in the same way as the O–C–O–H angle for HCOOH. In the cis isomers, the dihedral angle is 180.0°, whereas for the trans isomers it is 0.0°. Both are connected through a transition structure (TS) with a dihedral angle of 89.6° and 94.3° for HC(O)SH and HCOOH, respectively (see Fig. 1).

The values of these degrees of freedom in the transition structures indicate that the geometry of the TS for the HC(O)SH acid is slightly closer to that of the t-HC(O)SH isomer, whereas the TS of the HCOOH acid is closer to that of the c-HCOOH isomer. The energy barrier (with inclusive anharmonic ZPE) relative to the cis isomer is 7.94 and 7.33 kcal mol^{-1} for HC(O)SH and HCOOH, respectively. Both energy barriers are similar. However, the imaginary frequency of the saddle points associated with the reaction coordinate is 216.7 cm^{-1} higher for HCOOH. The latter indicates that the mass of the atom that holds the acidic hydrogen is of relevance in the isomerization reaction.

The relative electronic energy between the two isomers of HC(O)SH is 0.68 kcal mol^{-1}, which is notably smaller than that found for HCOOH (4.04 kcal mol^{-1}). These energy differences are due to the dipolar moments of the isomers. For instance, the difference between the dipolar moments of the isomers are 1.39 and 2.39 Debye for HC(O)SH and HCOOH respectively, with the most polar being the cis isomers. To easily visualize this, we built the electrostatic potential (ESP) maps of the isomers for both compounds (Fig. 2a). The polarization of the X–H bond (X being S for HC(O)SH and O for the HCOOH) has an important influence on the polarity of these molecules. The electrostatic potential (ESP) maps of the c-HC(O)SH and t-HC(O)SH isomers are very similar. However, for HCOOH, the differences in the charge distribution between cis and trans isomers are noticeable. This high charge polarization for c-HCOOH makes it unstable under the low pressure conditions of the ISM, because there is not any molecule close enough to this dipole to interact with and stabilize it. The latter statement has been checked by optimizing c-HCOOH and t-HCOOH in water using the continuum solvation model SMD (Marenich et al. 2009a,b). The derived electronic energy difference between the isomers is 0.5 kcal mol^{-1}. Although these interactions seem to be determinant in the relative stability of the isomers, the energy differences are also related to the delocalization energies. The second-order perturbative analysis for the cis and trans isomers of both acids shows that the strongest orbital interaction is between the lone pair of the sulfur and oxygen atoms that hold the hydrogen (LP orbital) with the π antibonding of the C–O (π^*_{CO}) (see Fig. 2b). In both cases, the highest delocalization energy is for the trans isomers, especially for HCOOH.

3.2. Kinetic results of the isomerizations

The analysis of the vibrational frequencies along the MEP for these isomerization transformations shows that variational effects should be negligible because the frequencies remain almost constant along the MEP. This effect is reflected in the relation $K^{\mathrm{CVT}}/K^{\mathrm{TST}}$, which is equal to 1 over the whole range of temperatures between 10 and 400 K.

An important factor limiting the accuracy of the theoretically computed rate constants at low temperatures is the high-frequency anharmonicities (Zheng et al. 2014; Gao et al. 2018; Wu et al. 2020). We take the high-frequency anharmonicities into account by multiplying the ZPE by a scaling factor for the energy minima and along the whole reaction path (0.948 for HCOOH and 0.949 for HC(O)SH). This approximation is explained elsewhere (Gao et al. 2018).

The imaginary frequency associated with the reaction coordinate for the TS-HC(O)SH is 405.67i, whereas for TS-HCOOH it is 622.35i. This difference in the imaginary frequency can be visualized easily through the vibrationally adiabatic potentials (V_{a}^{G}) depicted in Fig. 3: V_{a}^{G} is noticeably wider for HC(O)SH. The representative tunneling energies (RTEs) lie above the vibrational ground state ($v = 0$) of the cis isomers. The RTEs remain constant up to 60 K for HC(O)SH and 110 K for HCOOH due to the fact that the V_{a}^{G} potential is markedly narrower for HCOOH, and therefore the transmission probabilities are higher. These differences in V_{a}^{G} influence the cis to trans rate constants, K_1, especially at 10 K, where they are 3.73×10^{-21} for HCOOH and 6.04×10^{-26} for HC(O)SH. These rate constants suggest that this transformation is unlikely in the ISM at this low temperature.

When the RTE leaves the $v = 0$ of the cis isomer, there is a transition from the tunneling-controlled reactions to the thermally activated reactions, which can be seen in Fig. 3 as a change of the slope of the Arrhenius plots. There is a contribution from quantum tunneling up to approximately 110 K for HC(O)SH and 280 K for HCOOH. The contribution of tunneling to higher temperatures for HCOOH acid with respect to HC(O)SH is also a consequence of the V_{a}^{G} width.

From Fig. 3, we also find that the backward isomerization reactions (from trans to cis) are very different for the two species at very low temperatures (see rate constant values in Table 1). As the RTE lies in the ground state of the cis isomer, the trans conformer of HC(O)SH has to overcome an energy gap of ~0.64 kcal mol^{-1}, whereas the gap is of ~4.04 kcal mol^{-1} for HCOOH. This means that the ratio between the forward

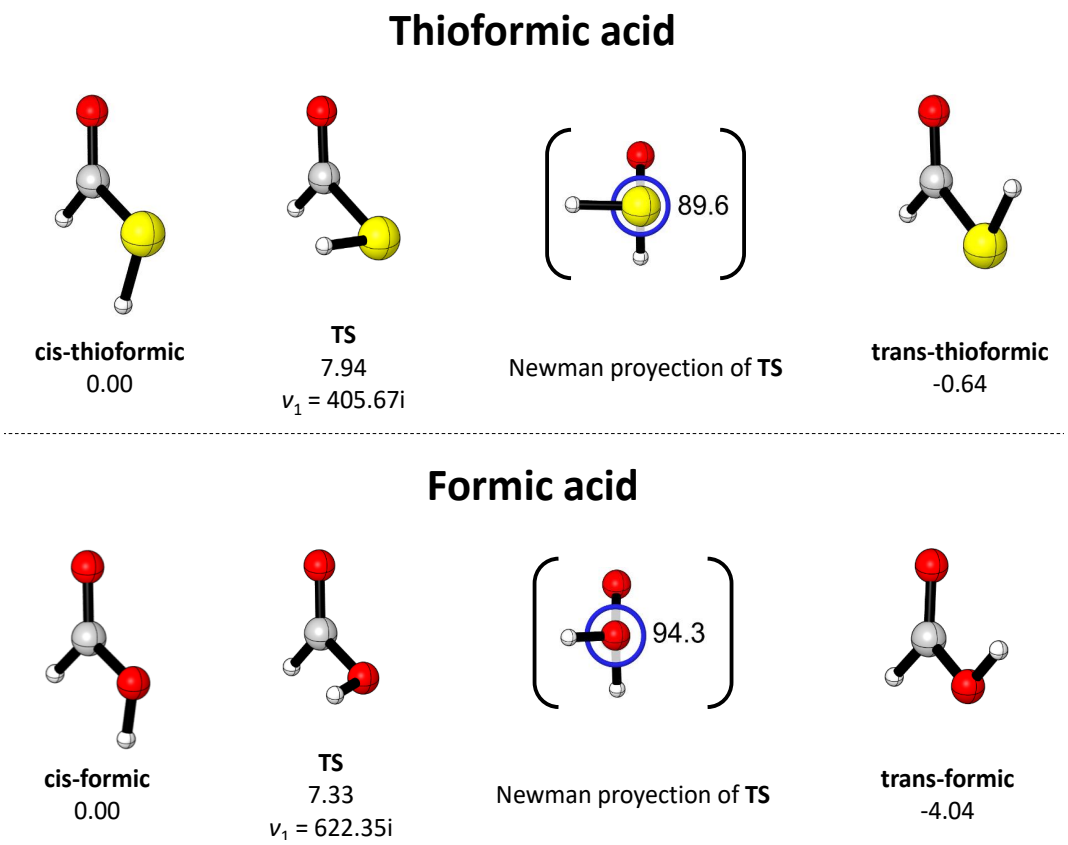

Fig. 1. Optimized structures of the cis, trans, and TS of HC(O)SH and HCOOH. Relative energies with respect the cis isomer calculated with the CCSD(T)-F12 method on the B2PLYP-D3(BJ) geometries are given, including anharmonic zero-point energies computed with the B2PLYP-D3(BJ) method.

and backward rate constants is 2.09×10^{88} for HCOOH and 1.17×10^{14} for HC(O)SH at 10 K. Even so, the backward isomerizations can be viable at high temperatures for both acids thanks to ground-state quantum tunneling. The contribution of tunneling to the rate constant in the backward isomerizations is noticeable up to the same temperatures as those for the forward paths.

4. Comparison with observations from the GUAPOS spectral survey

The results presented in the previous section suggest that we should not expect to detect the cis isomer of HCOOH due to isomerization in the ISM because of the large ratios between the rate constants of the forward (cis to trans) and backward (trans to cis) reactions for this acid at all temperatures. On the other hand, for HC(O)SH, this would only be true at low temperatures, because the ratio between the rate constants of the forward (cis to trans) and backward (trans to cis) reactions becomes $\leq$10 for temperatures $\geq$150 K. In this section, we analyze the data from the GUAPOS spectral survey (Mininni et al. 2020), and compare them to data found in the literature in order to investigate whether the trans/cis abundance ratios of HCOOH and HC(O)SH follow the values found for tunneling and are consistent with the expected ones under thermodynamic equilibrium, as proposed in Sect. 3.

We search for the trans and cis forms of both HCOOH and HC(O)SH acid towards the hot molecular core (HMC) G31 using data from the GUAPOS spectral survey (Mininni et al. 2020; Colzi et al. 2021). G31 is located at a distance of 3.75 kpc (Immer et al. 2019), with a luminosity of $\sim 4.5 \times 10^4\, L_\odot$ (from Osorio et al. 2009) and a mass of $\sim 70\, M_\odot$ (Cesaroni 2019). It harbors at least four massive star-forming cores towards its center (Beltrán et al. 2021). Moreover, different molecular lines present an inverse P Cygni profile, indicating that the core is collapsing (e.g., Girart et al. 2009; Beltrán et al. 2018). The core is also rotating as indicated by a clear NE–SW velocity gradient observed in different high-density tracers (e.g., Beltrán et al. 2004, 2018). Towards G31, many molecules have been detected (Beltrán et al. 2005, 2009, 2018; Rivilla et al. 2017b; Mininni et al. 2020; Gorai et al. 2021; Colzi et al. 2021), some of which are complex (>5 atoms). Therefore, G31 is a promising target to search for HCOOH and HC(O)SH.

The GUAPOS spectral survey was carried out with ALMA during Cycle 5 (project 2017.1.00501.S, P.I.: M. T. Beltrán) in band 3 with a frequency coverage from 84.05 GHz up to 115.91 GHz. The frequency resolution of the observation was 0.49 MHz, corresponding to a velocity resolution of $\sim$1.6 km s^{-1} at 90 GHz. The final angular resolution of the observations was $\sim 1\farcs2$ ($\sim$4500 au). The central coordinates were $\alpha_{J2000} = 18^h47^m34^s$ and $\delta_{J2000} = -0.1°12'45''$. The uncertainties in the flux calibration were of $\sim$5%. An additional error of 11% should also be considered due to the determination of the continuum level. For more details see Mininni et al. (2020) and Colzi et al. (2021).

The identification of the transitions of the cis and trans isomers of HCOOH and HC(O)SH in the GUAPOS spectrum was performed using version 01/12/2020 of the SLIM (Spectral Line Identification and Modeling) tool within the MADCUBA

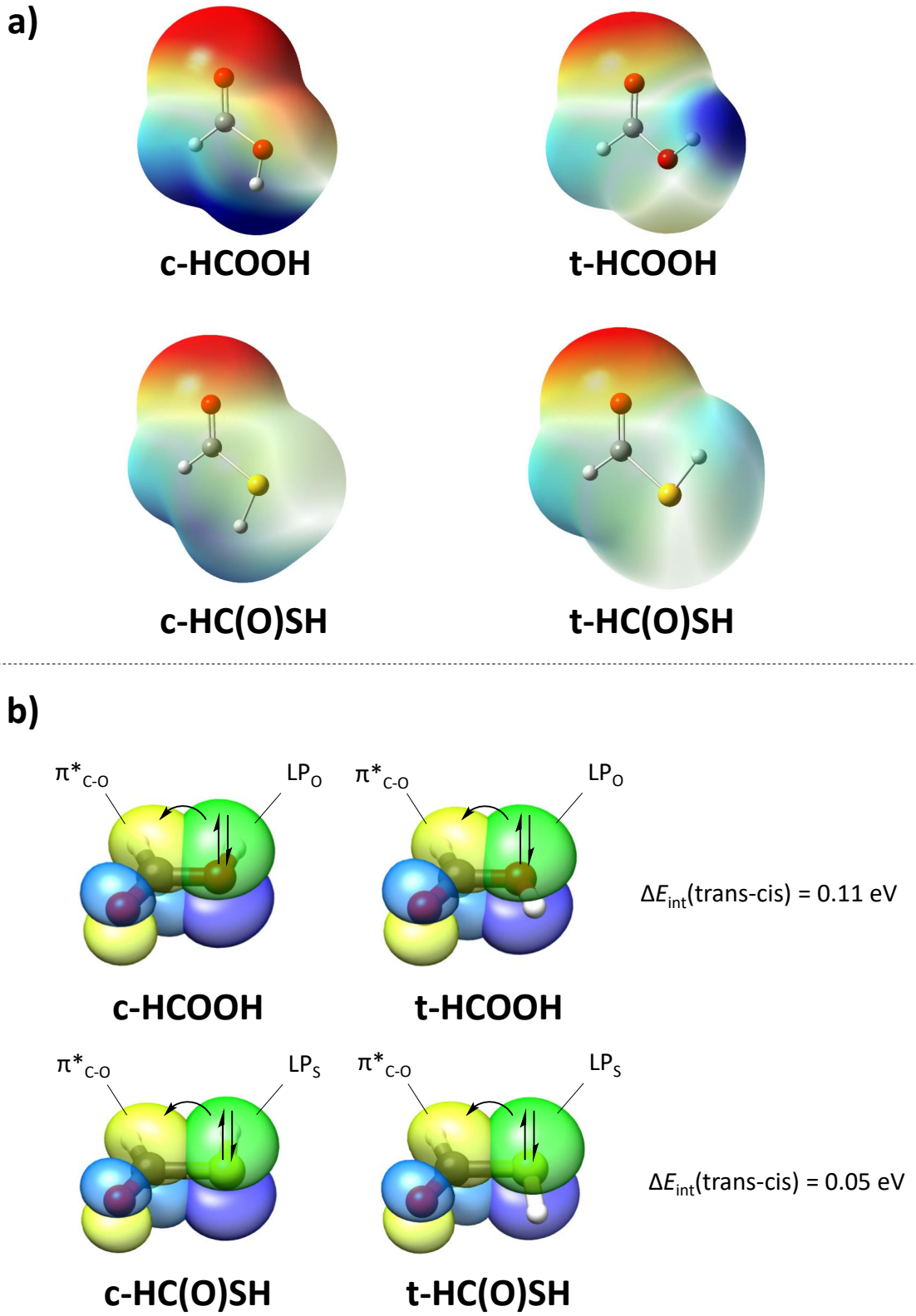

Fig. 2. Representation of isosurfaces for the acids HCOOH and HC(O)SH. (*a*) ESP isosurfaces of both isomers of HCOOH and HC(O)SH with isovalues between −0.04 and 0.05 au. The red and blue areas of the ESP maps represent the highest and lowest electron densities. (*b*) Isosurfaces of the π^*_{CO} and LP_S and LP_O orbitals for both isomers and interaction energy between these two orbitals due to delocalization.

package[1] (Martín et al. 2019). SLIM uses the spectroscopic entries from the Cologne Database for Molecular Spectroscopy[2] (CDMS, Müller et al. 2001, 2005; Endres et al. 2016) and the Jet

[1] Madrid Data Cube Analysis on ImageJ is a software developed at the Center of Astrobiology (CAB) in Madrid; https://cab.inta-csic.es/madcuba/

[2] http://cdms.astro.uni-koeln.de/classic/

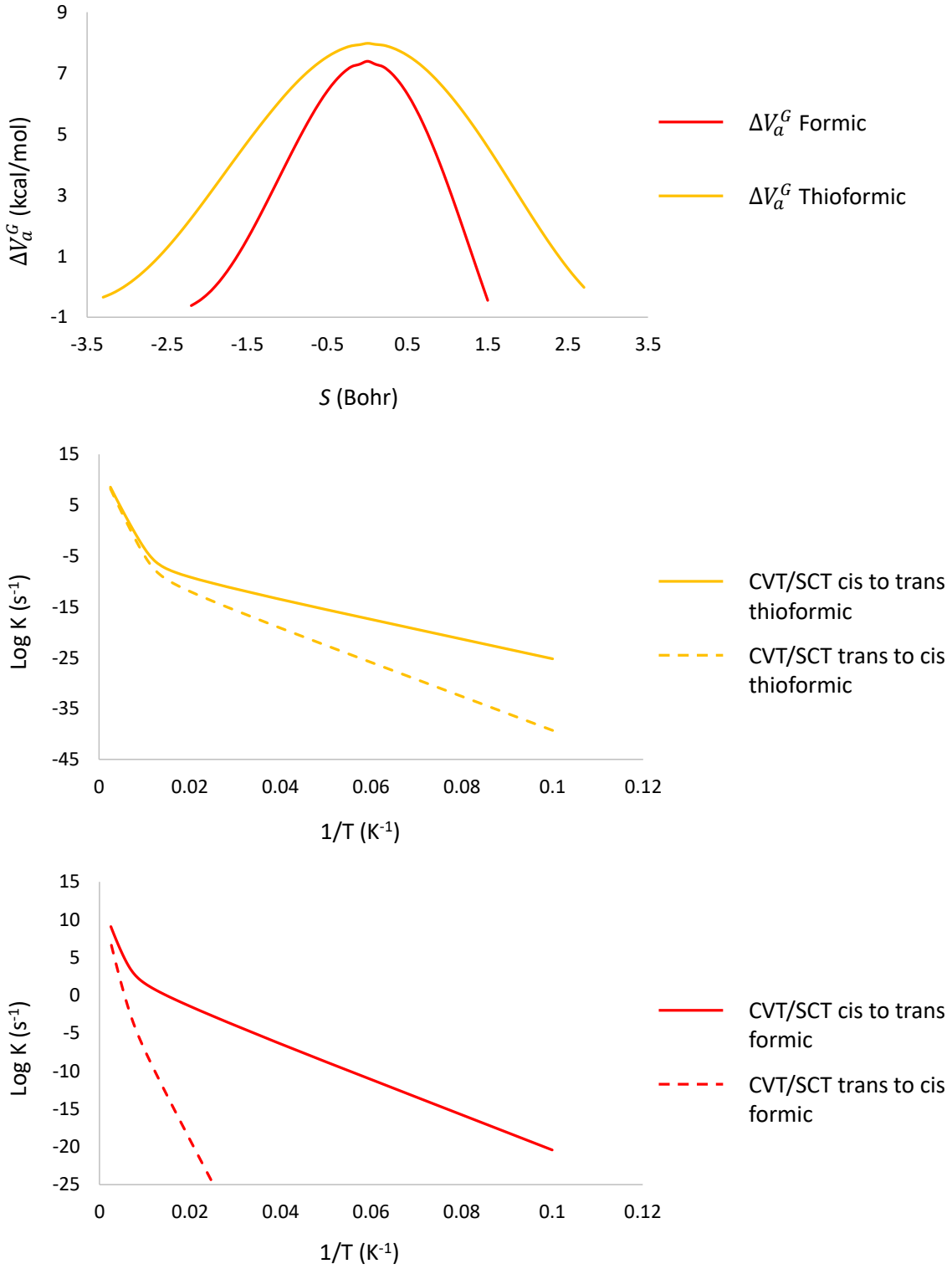

Fig. 3. Relative V_a^G potentials with respect the cis isomers in kcal mol^{-1}. Arrhenius plots for the cis to trans (solid lines) and trans to cis (dotted lines) isomerization reactions calculated with the CVT/SCT theory.

Propulsion Laboratory[3] (JPL, Pickett et al. 1998), and generates a synthetic spectrum, assuming local thermodynamic equilibrium (LTE) conditions and taking into account the line opacity. For each molecular species, we used the MADCUBA-AUTOFIT tool to compare the observed spectrum with the LTE synthetic one. This tool takes into account four physical parameters to create a synthetic LTE line profile: the column density (N), the excitation temperature (T_{ex}), peak radial velocity (v_{LSR}), and the full width half maximum (FWHM). The LTE assumption is well justified given the high volume density of the source $n(H_2)$ $\sim 10^8$ cm^{-3} (Mininni et al. 2020). The parameters are left free to obtain the best-LTE fit. When convergence is not reached, the parameters FWHM, v_{LSR}, and/or T_{ex} are fixed. The best-LTE fit of the

[3] https://spec.jpl.nasa.gov/ftp/pub/catalog/catdir.html

Table 1. CVT/SCT rate constants (in s^{-1}) for the cis to trans and trans to cis isomerization reactions of thioformic [HC(O)SH] and formic acids [HC(O)OH] and trans/cis ratios.

T (K)	Thioformic acid [HC(O)SH]			Formic acid [HC(O)OH]		
	$K^{CVT/SCT}$ [cis to trans]	$K^{CVT/SCT}$ [trans to cis]	K_1/K_{-1}	$K^{CVT/SCT}$ [cis to trans]	$K^{CVT/SCT}$ [trans to cis]	K_1/K_{-1}
10	6.04E−26	5.14 E−40	1.17E+14	3.73E−21	1.79E−109	2.09E+88
20	3.03E−16	2.78E−23	1.09E+07	1.67E−09	1.14E−53	1.47E+44
30	7.34E−13	1.49E−17	4.93E+04	1.64E−05	5.82E−35	2.82E+29
40	4.74E−11	1.43E−14	3.32E+03	1.89E−03	1.53E−25	1.23E+22
50	7.65E−10	1.17E−12	6.57E+02	3.65E−02	7.70E−20	4.74E+17
60	7.04E−09	3.16E−11	2.23E+02	2.89E−01	5.36E−16	5.40E+14
70	6.04E−08	5.85E−10	1.03E+02	1.39E+00	3.26E−13	4.26E+12
80	7.31E−07	1.26E−08	5.78E+01	4.93E+00	4.37E−11	1.13E+11
90	1.44E−05	3.90E−07	3.69E+01	1.46E+01	2.18E−09	6.70E+09
100	3.23E−04	1.26E−05	2.57E+01	3.88E+01	5.54E−08	7.00E+08
110	5.90E−03	3.09E−04	1.91E+01	9.82E+01	8.91E−07	1.10E+08
120	7.81E−02	5.23E−03	1.49E+01	2.47E+02	1.05E−05	2.36E+07
130	7.55E−01	6.24E−02	1.21E+01	6.36E+02	9.93E−05	6.41E+06
140	5.53E+00	5.47E−01	1.01E+01	1.68E+03	8.00E−04	2.09E+06
150	3.20E+01	3.71E+00	8.64E+00	4.45E+03	5.60E−03	7.94E+05
160	1.52E+02	2.02E+01	7.53E+00	1.16E+04	3.42E−02	3.40E+05
170	6.08E+02	9.12E+01	6.67E+00	2.93E+04	1.82E−01	1.61E+05
180	2.11E+03	3.52E+02	5.99E+00	7.02E+04	8.50E−01	8.26E+04
190	6.47E+03	1.19E+03	5.43E+00	1.60E+05	3.51E+00	4.55E+04
200	1.79E+04	3.59E+03	4.97E+00	3.43E+05	1.29E+01	2.66E+04
220	1.05E+05	2.45E+04	4.27E+00	1.36E+06	1.29E+02	1.05E+04
240	4.63E+05	1.23E+05	3.77E+00	4.47E+06	9.23E+02	4.84E+03
260	1.64E+06	4.86E+05	3.38E+00	1.26E+07	5.02E+03	2.51E+03
280	4.90E+06	1.59E+06	3.08E+00	3.12E+07	2.18E+04	1.43E+03
300	1.27E+07	4.47E+06	2.84E+00	6.94E+07	7.92E+04	8.76E+02
320	2.94E+07	1.11E+07	2.65E+00	1.41E+08	2.47E+05	5.70E+02
340	6.18E+07	2.48E+07	2.49E+00	2.66E+08	6.81E+05	3.91E+02
360	1.20E+08	5.09E+07	2.35E+00	4.70E+08	1.69E+06	2.79E+02
380	2.18E+08	9.71E+07	2.24E+00	7.87E+08	3.82E+06	2.06E+02
400	3.72E+08	1.74E+08	2.14E+00	1.26E+09	8.00E+06	1.57E+02

GUAPOS spectrum considering all molecular species analyzed so far within the survey can be found in Appendix E of Colzi et al. (2021).

5. Discussion

5.1. Isomerization of formic acid, HCOOH, in the ISM

The spectroscopy of t-HCOOH and c-HCOOH is taken from Winnewisser et al. (2002) and their dipole moments were measured by Kuze et al. (1982) for t-HCOOH and Hocking (1976) for c-HCOOH. The non-contaminated transitions used to fit the molecular lines of t-HCOOH within SLIM are listed in Table 2. Unfortunately, non-contaminated transitions of c-HCOOH have not been found.

Figure 4 shows the non-contaminated transitions used to fit t-HCOOH. To perform the fit we fixed the v_{LSR} to 96.5 km s^{-1}, which is the velocity of the source. The best-fit parameters obtained with MADCUBA are $T_{ex} = 152 \pm 45$ K, $FWHM = 8.0 \pm 0.3$ km s^{-1}, and $N = (1.4 \pm 0.6) \times 10^{17}$ cm^{-2}. This implies an abundance of $X = (1.4 \pm 0.7) \times 10^{-8}$ for the H_2 column density of $N_{H_2} = (1.0 \pm 0.2) \times 10^{25}$ cm^{-2} measured by Mininni et al. (2020) at 3 mm. On the other hand, c-HCOOH has not been detected and hence we derived a rough estimate of the upper limit of the column density using MADCUBA-SLIM, given the difficulty of obtaining a precise result due to the blending with lines of other species. Thus, we assumed T_{ex}, v_{LSR} and FWHM derived for t-HCOOH, and increased N to the maximum value compatible with the observed spectrum. Finally, we obtained $N \leq 1.6 \times 10^{15}$ cm^{-2}. This column density translates into an upper limit to the molecular abundance of c-HCOOH of $X \leq 1.6 \times 10^{-10}$. The trans/cis ratio measured toward G31 is thus ≥90. We note that if we use other T_{ex} ranging from 50 up to 300 K, we still get a trans/cis lower limit between ≥70 and ≥95.

In Table 3, we compare our G31 results with the trans/cis abundance ratio measured toward other astronomical sources. These sources range from cold cores such as B5 and L483 (with temperatures ∼5–15 K; Taquet et al. 2017; Agúndez et al. 2019), to massive hot cores (as e.g., G31 and W51 e2, with temperatures ∼100–200 K; see this work and Rivilla et al. 2017b), and the quiescent giant molecular cloud, G+0.693-0.027, located in the Galactic center (with temperatures between 70 and 150 K; see Rodríguez-Almeida et al. 2021). From this table, we find that the trans/cis ratios measured toward massive hot cores and the G+0.693-0.027 Galactic center molecular cloud are consistent with the small amount of c-HCOOH expected under thermodynamic equilibrium (Table 1), which makes it undetectable even at high temperatures.

However, at low temperatures, the predicted trans/cis ratios differ from those measured in the cold molecular cores B5 and L483 – by multiple orders of magnitude – where the trans/cis ratios found for HCOOH are 15 and 17, respectively. Indeed,

Table 2. Unblended or slightly blended transitions of the molecules studied in this work.

Molecule	Frequency (MHz)	Transition (J, K_a, K_c)	log I (nm^2 MHz)	E_{up} (K)	τ
t-HCOOH	86546.1891	4,1,4–3,1,3	−4.3888	13.57	0.12±0.08
t-HCOOH	89579.1785	4,0,4–3,0,3	−4.3269	10.77	0.13 ± 0.09
t-HCOOH	89861.4843	4,2,3–3,2,2	−4.4673	23.51	0.09 ± 0.06
t-HCOOH	90164.6296	4,2,2–3,2,1	−4.4644	23.53	0.09 ± 0.06
t-HCOOH	93098.3627	4,1,3–3,1,2	−4.3263	14.36	0.13 ± 0.09
t-HCOOH	108126.7202	5,1,5–4,1,4	−4.095	18.76	0.18 ± 0.12
t-HCOOH	111746.7845	5,0,5–4,0,4	−4.0451	16.13	0.20 ± 0.14
t-HCOOH	112287.1447	5,2,4–4,2,3	−4.1347	28.90	0.16 ± 0.10
t-HCOOH	112432.2921	5,4,2–4,4,1	−4.5567	67.06	0.05 ± 0.03
t-HCOOH	112432.3191	5,4,1–4,4,0	−4.5567	67.06	0.05 ± 0.03
t-HCOOH	112459.6214	5,3,3–4,3,2	−4.2744	44.81	0.11 ± 0.07
t-HCOOH	112467.0074	5,3,2–4,3,1	−4.2744	44.81	0.11 ± 0.07
t-HCOOH	112891.4435	5,2,3–4,2,2	−4.1301	28.95	0.16 ± 0.10
t-HC(O)SH	93208.624	8,0,8–7,0,7	−4.3707	20.17	0.016 ± 0.003
t-HC(O)SH	93589.887	8,5,4–7,5,3	−4.6797	87.60	0.0065 ± 0.0011
t-HC(O)SH	93589.887	8,5,3–7,5,2	−4.6797	87.60	0.0065 ± 0.0011
t-HC(O)SH	93592.509	8,4,5–7,4,4	−4.5544	63.35	0.0093 ± 0.0016
t-HC(O)SH	93592.509	8,4,4–7,4,3	−4.5544	63.35	0.0093 ± 0.0016
t-HC(O)SH	93592.808	8,6,2–7,6,1	−4.8664	117.22	0.0038 ± 0.0007
t-HC(O)SH	93592.808	8,6,3–7,6,2	−4.8664	117.22	0.0038 ± 0.0007
t-HC(O)SH	102631.9508	9,1,9–8,1,8	−4.2512	27.34	0.019 ± 0.003
t-HC(O)SH	105315.909	9,3,7–8,3,6	−4.3065	49.54	0.015 ± 0.003
t-HC(O)SH	105324.697	9,3,6–8,3,5	−4.3065	49.54	0.015 ± 0.003
t-HC(O)SH	105663.246	9,2,7–8,2,6	−4.2551	36.10	0.018 ± 0.003
t-HC(O)SH	107620.9874	9,1,8–8,1,7	−4.2115	28.54	0.020 ± 0.003
c-HC(O)SH	84566.811	11,0,11–10,1,10	−4.1819	36.99	0.0072 ± 0.0018
c-HC(O)SH	85979.209	13,1,12–13,0,13	−3.9382	55.05	0.012 ± 0.003
c-HC(O)SH	91058.108	14,1,13–14,0,14	−3.8857	63.09	0.012 ± 0.003
c-HC(O)SH	93801.341	8,3,5–7,3,4	−4.2206	44.91	0.0058 ± 0.0015
c-HC(O)SH	94030.48	8,2,6–7,2,5	−4.1609	31.24	0.0069 ± 0.0017
c-HC(O)SH	96658.0938	15,1,14–15,0,15	−3.8353	71.69	0.012 ± 0.003
c-HC(O)SH	99993.1226	19,1,18–18,2,17	−4.189	111.77	0.0047 ± 0.0012
c-HC(O)SH	107813.858	9,1,8–8,1,7	−3.9641	28.63	0.010 ± 0.002

Notes. The first column indicates the molecule for which the transitions are listed. The second column shows the frequency of the rotational transition given in the third column. Log I is the base 10 logarithm of the integrated intensity at 300 K, E_{up} is the energy of the upper level and τ is the optical depth of the transition derived from the LTE fit, as described in Sect. 4.

Table 3. Trans/cis ratio for HCOOH derived in the ISM compared with those predicted by this work for isomerization reactions.

Source	T_{kin} [(a)] (K)	Observed trans/cis	Predicted trans/cis (K_1/K_{-1} at T_{kin})	Reference
Barnard 5	5–15	15	$>10^{50}$	(1)
L483	10	17	2×10^{88}	(2)
G31	150 [(b)]	≥90	8×10^{5}	(3)
G+0.693-0.027	150 [(c)]	≥125	8×10^{5}	(4)
W51 e2	90–180	≥16	7×10^{9}–8×10^{4}	(5)

Notes. [(a)] T_{kin} is the gas kinetic temperature of the source inferred from t-HCOOH. [(b)] This is an average kinetic temperature towards the G31 hot molecular core (e.g., Beltrán et al. 2018). [(c)] Inferred from CH_3CN data by Zeng et al. (2018).
References. (1) Taquet et al. (2017); (2) Agúndez et al. (2019); (3) This work; (4) Rodríguez-Almeida et al. (2021); (5) Rivilla et al. (2017b).

the isomerization of HCOOH acid should not occur at these low temperatures (see the low values for the K_1 and K_{-1} rate constant in Table 1 for $T \leq 30$ K). This implies that the ratios measured between the isomers of HCOOH at low temperatures must be due to competitive chemical processes and are not related to an isomerization transformation.

We note that we do not compare our results with the trans/cis ratios measured toward the Orion Bar because the

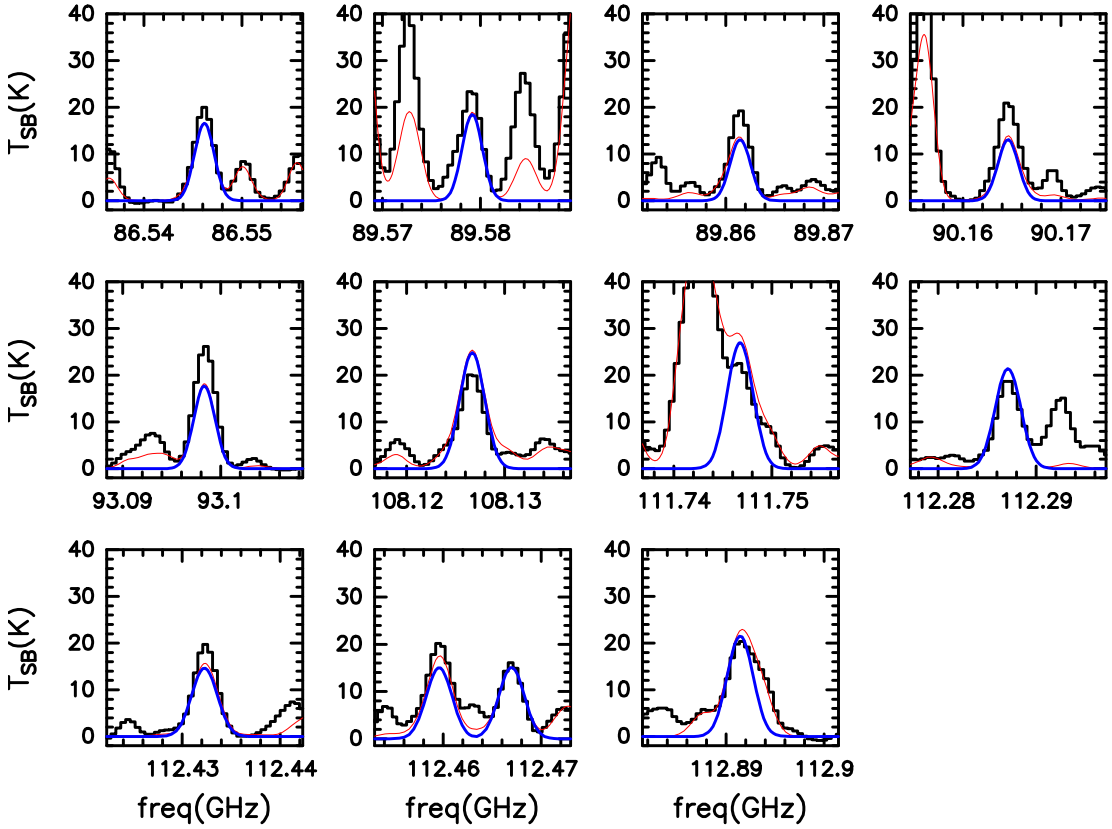

Fig. 4. Transitions listed in Table 2 and used to fit the trans isomer of HCOOH (t-HCOOH). The blue curve represents the best LTE fit obtained with MADCUBA and the red curve shows the simulated spectrum taking into account all the species identified in the region so far.

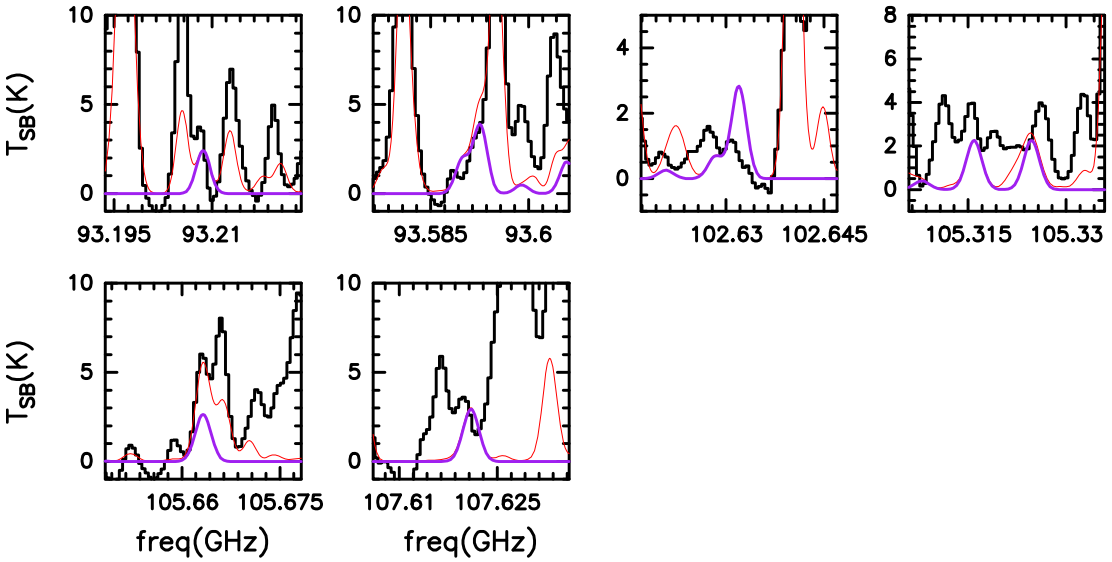

Fig. 5. Transitions listed in Table 2 and used to fit the trans form of HC(O)SH (t-HC(O)SH). The purple curve represents the best LTE fit obtained with MADCUBA and the red curve shows the simulated spectrum taking into account all the species identified in the region so far. We note that the discrepancy between the predicted and observed spectra at 102.63 GHz may be due to a poor baseline removal at this frequency range and/or to some absorption associated with the strong molecular line centered at 102.645 GHz.

production of c-HCOOH in this source is due to the gas being irradiated by *uv* photons (Cuadrado et al. 2016). This process enables photoisomerization processes by exciting molecules to higher electronic states, which is a completely different mechanism to that of the isomerization transformation through tunneling.

5.2. Isomerization of thioformic acid, HC(O)SH, in the ISM

As mentioned in the introduction, HC(O)SH acid has recently been reported in the ISM toward the Galactic center giant molecular cloud G+0.693-0.027 (Rodríguez-Almeida et al. 2021). In this section, we also search for this species in the G31 massive

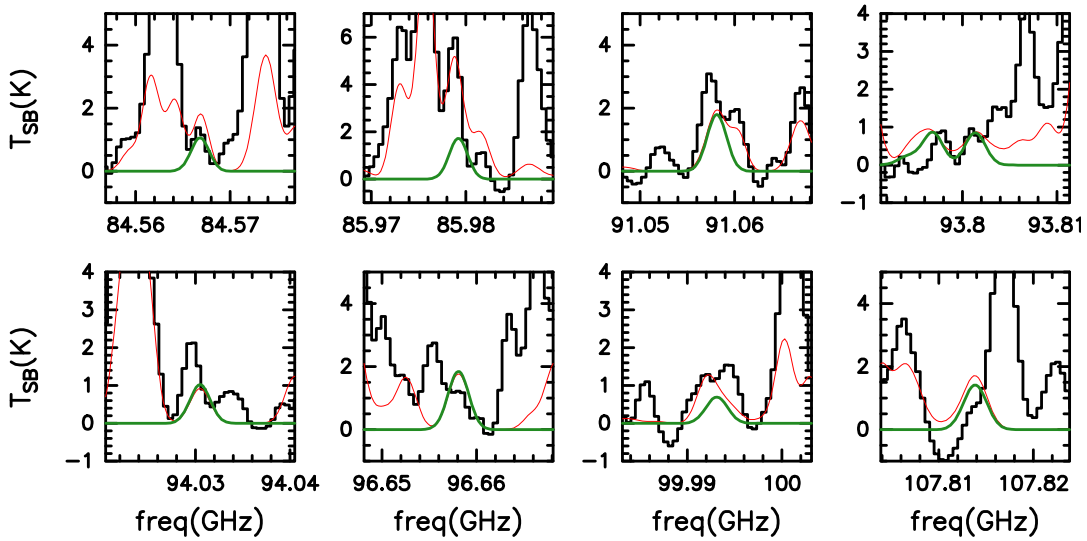

Fig. 6. Transitions listed in Table 2 and used to fit the cis form of HC(O)SH (c-HC(O)SH). The green curve represents the best LTE fit obtained with MADCUBA and the red curve shows the simulated spectrum taking into account all the species identified in the region so far.

Table 4. Trans/cis ratio for HC(O)SH derived in the ISM compared with those predicted by this work for isomerization reactions.

Source	$T_{kin}^{(a)}$ (K)	Observed trans/cis	Predicted trans/cis (K_1/K_{-1} at T_{kin})	Reference
G31	150 [(b)]	3.7 ± 1.5 [(c)]	8.6	(1)
G+0.693-0.027	150 [(d)]	≥5	8.6	(2)

Notes. [(a)] T_{kin} is the gas kinetic temperature of the source inferred from t-HCOOH. [(b)] This is an average kinetic temperature towards the G31 hot molecular core (e.g., Beltrán et al. 2018). [(c)]This ratio is obtained from two tentative detections and should be taken with caution. [(d)] Inferred from CH_3CN data by Zeng et al. (2018).
References. (1) This work; (2) Rodríguez-Almeida et al. (2021).

hot core making use of the GUAPOS spectral survey. For this, we used the spectroscopic information of t-HC(O)SH and c-HC(O)SH obtained by Hocking & Winnewisser (1976a) and the dipole moments measured by Hocking & Winnewisser (1976b). The noncontaminated transitions used to fit the molecular lines of t-HC(O)SH and c-HC(O)SH can also be found in Table 2.

The trans and cis forms of HC(O)SH are tentatively detected towards G31. Figures 5 and 6 report the less contaminated transitions of these species for which we derive a tentative N. For t-HC(O)SH the main contaminants are acetone (CH_3COCH_3) and ethylene glycol ($HOCH_2CH_2OH$) at 105.663 GHz and acetaldehyde (CH_3CHO) at 93.595 GHz. For these two lines, the total observed emission can be perfectly fitted taking into account the emission from t-HC(O)SH. The observed spectra at the frequencies of the remaining lines cannot be completely reproduced due to the contribution from unidentified species. The main contaminants for c-HC(O)SH are CH_3OCH_3 at 85.978 GHz, CH_3COOH at 85.981 GHz, CH_3CONH_2 at 84.567 GHz, and CH_3OCHO at 99.992 GHz. We fixed T_{ex}, v_{LSR}, and FWHM to those inferred for t-HCOOH and we obtained a $N = (2.0 \pm 0.5) \times 10^{16}$ cm^{-2} and an abundance of $X = (2.0 \pm 0.6) \times 10^{-9}$ for t-HC(O)SH, and a column density of $N = (5.4 \pm 1.5) \times 10^{15}$ cm^{-2} and an abundance of $X = (5.4 \pm 1.8) \times 10^{-10}$ for c-HC(O)SH. The resulting trans/cis ratio for HC(O)SH acid is 3.7 ± 1.5. We remind the reader that this value has been inferred from the ratio of two tentative detections and should be taken with caution.

In Table 4, we compare the G31 results with those obtained for G+0.693-0.027 and our kinetic results of Sect. 3. From this table, we find that the ratio of the rate constants between the forward (cis to trans) and backward (trans to cis) reactions are consistent with the trans/cis ratios measured toward both sources. In fact, assuming a kinetic temperature ≥240 K for G31 (Beltrán et al. 2018), the predicted K_1/K_{-1} (trans/cis) ratios fall below ∼4, which nicely matches the tentative trans/cis ratio measured toward G31 with the GUAPOS data. Therefore, the comparison of our kinetic results with observations suggests that c-HC(O)SH is likely present in hot environments where the isomerization transformation due to tunneling can take place.

6. Conclusions

In this work, we carried out a theoretical analysis of the cis-to-trans and trans-to-cis isomerization reactions of the HCOOH acid and of the recently detected HC(O)SH thioacid. The kinetic results show that the trans/cis ratio found in the ISM for both acids could follow a behavior typical of the thermodynamic equilibrium, independently of the formation route, thanks to ground-state quantum tunneling effects.

Our kinetic results reveal that, at very low temperatures, the isomerization reactions cannot occur because their rate constants are very low. This is in disagreement with the observed trans/cis ratios of HCOOH acid in the cold molecular cores B5 and L483, which implies that chemical processes such as competitive chemical routes or excitations caused by secondary uv fields must be responsible.

We also searched for these molecules in the context of the GUAPOS spectral survey obtained with the ALMA interferometer towards the hot core G31. We detect the trans form

of HCOOH and tentatively detected trans and cis HC(O)SH, the latter for the first time in the ISM. For the column density of c-HCOOH, we obtained an upper limit. At high temperatures, our theoretical predictions support the upper limits found for HCOOH acid in G31 (trans/cis ≥90), G+0.693-0.027 (trans/cis ≥125), and W51 e2 (trans/cis ≥16). The energy difference between the c-HCOOH and the more stable t-HCOOH causes the equilibrium to displace toward the latter. This phenomenon means that the amount of the c-HCOOH in the ISM is very low, and even undetectable in hot molecular clouds. For HC(O)SH acid, our tentative detections of both isomers toward G31 within the GUAPOS data provides a trans/cis ratio of 3.7±1.5, which is close to the ratio of the equilibrium constants computed at ≥240 K (≤4). Our quantum chemical calculations also support the upper limit measured for the trans/cis abundance ratio of HC(O)SH acid toward the G+0.693-0.027 molecular cloud (≥5).

Acknowledgements. J.G.d.l.C. acknowledges the Spanish State Research Agency (AEI) through project number MDM-2017-0737 Unidad de Excelencia "María de Maeztu"–Centro de Astrobiología (CSIC-INTA). J.C.C. acknowledges the Junta de Extremadura and European Regional Development Fund, Spain, Project No. GR18010. I.J.-S. and J.M.-P. have received partial support from AEI (PID2019-105552RB-C41). G.M. acknowledges the support of the Alexander von Humboldt Foundation through a postdoctoral research grant. V.M.R. and L.C. have received funding from the Comunidad de Madrid through the Atracción de Talento Investigador (Doctores con experiencia) Grant (COOL: Cosmic Origins Of Life; 2019-T1/TIC-15379). C. M. acknowledges funding from the European Research Council (ERC) under the European Union's Horizon 2020 program, through the ECOGAL Synergy grant (grant ID 855130). This paper makes use of the following ALMA data: ADS/JAO.ALMA#2017.1.00501.S. ALMA is a partnership of ESO (representing its member states), NSF (USA) and NINS (Japan), together with NRC (Canada), MOST and ASIAA (Taiwan), and KASI (Republic of Korea), in cooperation with the Republic of Chile. The Joint ALMA Observatory is operated by ESO, AUI/NRAO and NAOJ. Computational assistance was provided by the Supercomputer facilities of LUSITANIA founded by Cénits and Computaex Foundation.

References

Adler, T. B., Knizia, G., & Werner, H.-J. 2007, J. Chem. Phys., 127, 221106
Agúndez, M., Marcelino, N., Cernicharo, J., Roueff, E., & Tafalla, M. 2019, A&A, 625, A147
Baiano, C., Lupi, J., Tasinato, N., Puzzarini, C., & Barone, V. 2020, Molecules, 25
Balucani, N., Skouteris, D., Ceccarelli, C., et al. 2018, Mol. Astrophys., 13, 30
Bao, J. L., & Truhlar, D. G. 2017, Chem. Soc. Rev., 46, 7548
Barone, V. 2004, JChPh, 120, 3059
Belloche, A., Müller, H. S. P., Menten, K. M., Schilke, P., & Comito, C. 2013, A&A, 559, A47
Beltrán, M. T., Cesaroni, R., Neri, R., et al. 2004, ApJ, 601, L187
Beltrán, M. T., Cesaroni, R., Neri, R., et al. 2005, A&A, 435, 901
Beltrán, M. T., Codella, C., Viti, S., Neri, R., & Cesaroni, R. 2009, ApJ, 690, L93
Beltrán, M. T., Cesaroni, R., Rivilla, V. M., et al. 2018, A&A, 615, A141
Beltrán, M. T., Rivilla, V. M., Cesaroni, R., et al. 2021, A&A, 648, A100
Bizzocchi, L., Prudenzano, D., Rivilla, V. M., et al. 2020, A&A, 640, A98
Cesaroni, R. 2019, A&A, 631, A65
Chuang, Y. Y., Corchado, J. c., & Truhlar, D. G. 1999, J. Phys. Chem. A, 103, 1140
Colzi, L., Rivilla, V. M., Beltrán, M. T., et al. 2021, A&A, 653, A129
Cuadrado, S., Goicoechea, J. R., Roncero, O., et al. 2016, A&A, 596, L1
Domanskaya, A., Marushkevich, K., Khriachtchev, L., & Räsänen, M. 2009, J. Chem. Phys., 130, 154509
Dunning Jr., T. H. 1989, J. Chem. Phys., 90, 1007
Endres, C. P., Schlemmer, S., Schilke, P., Stutzki, J., & Müller, H. S. P. 2016, J. Mol. Spectro., 327, 95
Favre, C., Fedele, D., Semenov, D., et al. 2018, ApJ, 862, L2
Ferro-Costas, D., Truhlar, D. G., & Fernández-Ramos, A. 2020, Pilgrim-version 2020.2 (University of Minneapolis, Minnesota, MN, and Universidade de Santiago de Compostela, Spain)
Feyereisen, M., Fitzerald, G., & Komornicki, A. 1993, Chem. Phys. Lett., 208, 359
Frisch, M. J. et al. 2016, Gaussian 16 Revision A.03
Gao, L. G., Fernández-Ramos, A., & Truhlar, D. G. 2018, J. Am. Chem. Soc., 140, 2906
García de la Concepción, J., Jiménez-Serra, I., Corchado, J. C., Rivilla, V. M., & Martín-Pintado, J. 2021, ApJ, 912, L6
Gieser, C., Semenov, D., Beuther, H., et al. 2019, A&A, 631, A142
Girart, J. M., Beltrán, M. T., Zhang, Q., Rao, R., & Estalella, R. 2009, Science, 324, 1408
Gorai, P., Das, A., Shimonishi, T., et al. 2021, ApJ, 907, 108
Grimme, S. 2006, J. Chem. Phys., 124, 034108
Grimme, S., Antony, J., Ehrlich, S., & Krieg, H. 2010, J. Chem. Phys., 132, 154104
Grimme, S., Ehrlich, S., & Goerigk, L. 2011, J. Comput. Chem., 32, 1456
Hocking, W. H. 1976, Z. Naturforsch. A, 31, 1113
Hocking, W. H., & Winnewisser, G. 1976a, Z. Naturforsch. A, 31, 422
Hocking, W., & Winnewisser, G. 1976b, Z. Naturfor. A J. Phys. Sci., 31, 995
Immer, K., Li, J., Quiroga-Nuñez, L. H., et al. 2019, A&A, 632, A123
Kendall, R. A., Dunning Jr, T. H., & Harrison, R. J. 1992, J. Chem. Phys., 96, 6796
Knizia, G., Adler, T. B., & Werner, H.-J. 2009, J. Chem. Phys., 130, 054104
Kuze, H., Kuga, T., & Shimizu, T. 1982, J. Mol. Spectro., 93, 248
Lattanzi, V., Bizzocchi, L., Vasyunin, A. I., et al. 2020, A&A, 633, A118
Lee, C.-F., Codella, C., Li, Z.-Y., & Liu, S.-Y. 2019, ApJ, 876, 63
Legault, C. Y. 2009, `http://www.cylview.org`
Li, J., Wang, J., Qiao, H., et al. 2020, MNRAS, 492, 556
Lignell, A., Osadchuk, I., Räsänen, M. & Lundell, J. 2021, ApJ, 917, 68
Loomis, R. A., Zaleski, D. P., Steber, A. L., et al. 2013, ApJ, 765, L9
Lupi, J., Puzzarini, C., & Barone, V. 2020, ApJ, 903, L35
Maçôas, E. M. S., Khriachtchev, L., Pettersson , M., Fausto , R., & Räsänen, M. 2005, Phys. Chem. Chem. Phys., 7, 743
Manigand, S., Jørgensen, J. K., Calcutt, H., et al. 2020, A&A, 635, A48
Marenich, A. V., Cramer, C. J., & Truhlar, D. G. 2009a, J. Chem. Phys. B, 113, 4538
Marenich, A. V., Cramer, C. J., & Truhlar, D. G. 2009b, J. Chem. Phys. B, 113, 6378
Martín, S., Martín-Pintado, J., Blanco-Sánchez, C., et al. 2019, A&A, 631, A159
Maureira, M. J., Pineda, J. E., Segura-Cox, D. M., et al. 2020, ApJ, 897, 59
Melli, A., Melosso, M., Tasinato, N., et al. 2018, ApJ, 855, 123
Mininni, C., Beltrán, M. T., Rivilla, V. M., et al. 2020, A&A, 644, A84
Molpeceres, G., García de la Concepción, J. & Jiménez-Serra, I. 2021, ApJ, 923, 159
Müller, H. S. P., Thorwirth, S., Roth, D. A., & Winnewisser, G. 2001, A&A, 370, L49
Müller, H. S. P., Schlöder, F., Stutzki, J., & Winnewisser, G. 2005, J. Mol. Struct., 742, 215
Neese, F. 2012, WIREs: Comput. Mol., 2, 73
Neese, F., Wennmohs, F., Becker, U., & Riplinger, C. 2020, J. Chem. Phys., 152, 224108
Osorio, M., Anglada, G., Lizano, S., & D'Alessio, P. 2009, ApJ, 694, 29
Peng, Y., Rivilla, V. M., Zhang, L., Ge, J. X., & Zhou, B. 2019, ApJ, 871, 251
Pettersen, E. F., Goddard, T. D., Huang, C. C., et al. 2004, J. Comp. Chem., 25, 1605
Pettersson, M., Maçôas, E. M. S., Khriachtchev, L., et al. 2002, J. Chem. Phys., 117, 9095
Pickett, H. M., Poynter, R. L., Cohen, E. A., et al. 1998, J. Quant. Spectr. Rad. Transf., 60, 883
Puzzarini, C. 2015, J. Phys. Chem. A, 119, 11614
Quan, D., Herbst, E., Corby, J. F., Durr, A., & Hassel, G. 2016, ApJ, 824, 129
Rivilla, V. M., Beltrán, M. T., Martín-Pintado, J., et al. 2017a, A&A, 599, A26
Rivilla, V. M., Beltrán, M. T., Cesaroni, R., et al. 2017b, A&A, 598, A59
Rivilla, V. M., Martín-Pintado, J., Jiménez-Serra, I., et al. 2018, MNRAS, 483, L114
Rodríguez-Almeida, L. F., Jiménez-Serra, I., Rivilla, V. M., et al. 2021, ApJ, 912, L11
Shingledecker, C. N., Molpeceres, G., Rivilla, V. M., Majumdar, L., & Kästner, J. 2020, ApJ, 897, 158
Taquet, V., Wirström, E. S., Charnley, A., et al. 2017, A&A, 607, A20
Tsuge, M., & Khriachtchev, L. 2014, J. Phys. Chem. A, 119, 2628
van Gelder, M. L., Tabone, B., Tychoniec, Ł., et al. 2020, A&A, 639, A87
Vastel, C., Ceccarelli, C., Lefloch, B., & Bachiller, R. 2014, ApJ, 795, L2
Vazart, F., Calderini, D., Skouteris, D., Latouche, C., & Barone, V. 2015, J. Chem. Theory Comput., 11, 1165
Winnewisser, M., Winnewisser, B. P., Stein, M., et al. 2002, J. Mol. Spectr., 216, 259
Wu, J., Gao, L. G., Varga, 2020, Angew. Chem. Int. Ed., 59, 10826
Yang, Y.-L., Sakai, N., Zhang, Y., et al. 2021, ApJ, 910, 20
Zeng, S., Jiménez-Serra, I., Rivilla, V. M., et al. 2018, MNRAS, 478, 2962
Zheng, J., Meana-Paneda, R., & Truhlar, D. G. 2014, J. Am. Chem. Soc., 136, 5150

Appendix A: Comparison Between Coupled Cluster and Double-Hybrid Calculations

Table A.1 shows the relative electronic energies of the cis, trans, and saddle point for the isomerization of the HCOOH relative to the cis isomer. These results are obtained after a full geometry optimization with the selected methods. To characterize the nature of the stationary points, frequency calculations were also carried out at the same level of theory. Thus, for comparison, the harmonic zero-point energies are also given. The great agreement obtained between both methods indicates that this double hybrid is an excellent method for quantitative studies for this system. This agreement in the energies is a reflection of the similarity in the optimized geometries between both methods, which give almost the same results and are gathered in the Table A.2. As a complement of Table A.2, the Figure A.1 shows the atom numbering of the formic acid used in this table.

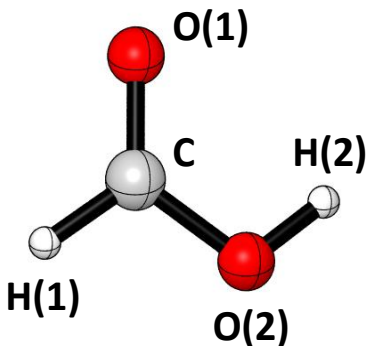

Fig. A.1. Atom numbering of HCOOH.

Table A.1. Relative electronic energies and harmonic ZPE of the cis, trans, and TS optimized geometries of HCOOH at CCSD(T)-F12 and B2PLYP-D3(BJ) level of theory

	B2PLYP-D3(BJ)[a]		CCSD(T)-F12[b]	
	ΔE	ZPE_{har}	ΔE	ZPE_{har}
cis	0.00	20.96	0.00	20.29
TS	8.77	19.90	8.39	20.02
trans	-4.15	21.18	-4.25	21.29

Notes. [a] In combination with the aug-cc-pVTZ basis set. [b] In combination with the cc-pVTZ-F12-CABS and cc-pVTZ-F12 basis set and the augmented aug-cc-pVTZ for correlation and coulomb fitting.

Table A.2. Geometrial parameters of the cis, trans, and TS optimized geometries of HCOOH at CCSD(T)-F12 and B2PLYP-D3(BJ) level of theory. Bond distances are given in angstroms and angles in degrees.

	cis		TS		trans	
	B2PLYP-D3(BJ)[a]	CCSD(T)-F12[b]	B2PLYP-D3(BJ)[a]	CCSD(T)-F12[b]	B2PLYP-D3(BJ)[a]	CCSD(T)-F12[b]
C-O(1)	1.19	1.19	1.19	1.19	1.20	1.20
C-O(2)	1.35	1.35	1.38	1.37	1.35	1.34
C-H(1)	1.10	1.10	1.10	1.10	1.09	1.09
O(2)-H(2)	0.96	0.96	0.96	0.96	0.97	0.97
O(1)-C-O(2)	122.40	122.30	123.77	123.60	125.07	124.91
C-O(2)-H(2)	109.70	109.21	111.49	110.57	107.30	106.74
H(1)-C-O(2)	113.53	113.70	112.51	112.80	109.73	109.98
H(1)-C-O(1)	124.07	124.00	123.60	123.49	125.20	125.11
H(2)-O(2)-C-H(1)	0.00	0.00	-89.64	-89.29	179.99	180.00
H(2)-O(2)-C-O(1)	180.00	180.00	94.27	94.33	0.01	0.00

Notes. [a] In combination with the aug-cc-pVTZ basis set. [b] In combination with the cc-pVTZ-F12-CABS and cc-pVTZ-F12 basis set and the augmented aug-cc-pVTZ for correlation and coulomb fitting.